Geochemistry Geophysics Geosystems G3
AN ELECTRONIC JOURNAL OF THE EARTH SCIENCES
Published by AGU and the Geochemical Society

Article
Volume 6, Number 7
26 July 2005
Q07010, doi:10.1029/2005GC000918
ISSN: 1525-2027

Modeling of acoustic wave dissipation in gas hydrate–bearing sediments

Gilles Guerin and David Goldberg

Borehole Research Group, Lamont-Doherty Earth Observatory, Route 9W, Palisades, New York 10964, USA (guerin@ldeo.columbia.edu; goldberg@ldeo.columbia.edu)

[1] Recent sonic and seismic data in gas hydrate–bearing sediments have indicated strong waveform attenuation associated with a velocity increase, in apparent contradiction with conventional wave propagation theory. Understanding the reasons for such energy dissipation could help constrain the distribution and the amounts of gas hydrate worldwide from the identification of low amplitudes in seismic surveys. A review of existing models for wave propagation in frozen porous media, all based on Biot's theory, shows that previous formulations fail to predict any significant attenuation with increasing hydrate content. By adding physically based components to these models, such as cementation by elastic shear coupling, friction between the solid phases, and squirt flow, we are able to predict an attenuation increase associated with gas hydrate formation. The results of the model agree well with the sonic logging data recorded in the Mallik 5L-38 Gas Hydrate Research Well. Cementation between gas hydrate and the sediment grains is responsible for the increase in shear velocity. The primary mode of energy dissipation is found to be friction between gas hydrate and the sediment matrix, combined with an absence of inertial coupling between gas hydrate and the pore fluid. These results predict similar attenuation increase in hydrate-bearing formations over most of the sonic and seismic frequency range.

Components: 8110 words, 7 figures, 1 table.

Keywords: attenuation; gas hydrates; sonic logging.

Index Terms: 0915 Exploration Geophysics: Downhole methods; 3004 Marine Geology and Geophysics: Gas and hydrate systems; 5144 Physical Properties of Rocks: Wave attenuation.

Received 12 January 2005; **Revised** 16 May 2005; **Accepted** 6 June 2005; **Published** 26 July 2005.

Guerin, G., and D. Goldberg (2005), Modeling of acoustic wave dissipation in gas hydrate–bearing sediments, *Geochem. Geophys. Geosyst.*, *6*, Q07010, doi:10.1029/2005GC000918.

1. Introduction

[2] Gas hydrates are crystalline molecular complexes formed from mixtures of water and suitably sized gas molecules, most commonly methane in the natural environment. Under proper high pressure and low temperature conditions, the water molecules form unstable lattice structures upon hydrogen bonding, with interstitial cavities that the gas molecules can occupy. When the gas supply is sufficient for a minimum number of cavities to be occupied, the crystalline structures become stable and solid gas hydrates can form [*Sloan*, 1990]. The thermodynamic conditions required for this process occur on most continental margins, and the carbon existing as gas hydrate is estimated to be on the order of 10,000 Gigatons, or equivalent to twice the amount of carbon found in other fossil fuels [*Kvenvolden*, 2002]. While the total estimates vary widely [*Kvenvolden*, 1999; *Milkov et al.*, 2003], it has been recognized that such quantities can have significant implications as a potential energy reserve, as a risk for margins stability, as the possible source for the release into the atmosphere of large quantities of methane, a potent greenhouse gas, and overall as an over-

looked major component of the global carbon cycle [*Henriet and Mienert*, 1998; *Kvenvolden*, 2002].

[3] With only few studies to date dedicated to natural gas hydrate, the global estimates are based on a few samples [*Milkov et al.*, 2003] and on the signature of the occurrence of gas hydrate in marine sediments worldwide: the presence of a Bottom Simulating Reflector (BSR). This reverse amplitude seismic reflector, subparallel to the seafloor, marks the bottom of the thermodynamic Gas Hydrate Stability field. It is generated by the velocity contrast between the high-velocity gas hydrate–bearing sediments above, and the low-velocity free-gas-bearing sediments below. The respective influence of the free gas and of gas hydrate on the occurrence of a BSR is still under debate [*Kvenvolden*, 1998], but BSRs have been identified on continental margins worldwide and their total coverage is the primary source for the global estimates of gas hydrate. However, while a BSR indicates the location of gas hydrate, it does not provide any information on the amounts of hydrate present in the overlying sediments. Such information could be provided by the waveform amplitudes in seismic surveys. Areas of low seismic amplitude, or "blanking," associated with the presence of gas hydrate, have been observed above some BSR [*Lee and Dillon*, 2001]. Low lithological variability in some hydrate deposits can contribute to the low reflectivity [*Holbrook et al.*, 1996], and the origin of the blanking is not fully understood, but the influence of gas hydrate on seismic amplitude is now recognized [*Lee and Dillon*, 2001; *Hornbach et al.*, 2003; *Dvorkin and Uden*, 2004]. The possibility to relate seismic amplitude to gas hydrate concentrations could greatly improve our capacity to estimate gas hydrate accumulations. While the vertical extent of the blanking is an indicator of the distribution of gas hydrate, the "intensity" of the blanking, directly related to seismic attenuation, could possibly allow quantification of the amounts of gas hydrate present. The observation of low sonic logging waveform amplitudes in hydrate-bearing sediments on the Blake Ridge during ODP Leg 164 [*Guerin et al.*, 1999] suggested that such relationship between gas hydrate and seismic amplitude could be understood by the careful analysis of sonic logging waveforms.

[4] Downhole measurements, or logs, are used to measure continuously and in situ the physical properties of the formation surrounding a borehole. Because of the instability of gas hydrate at surface conditions, logs are critical to the identification of its distribution. The measurements the most sensitive to the presence of gas hydrate are the resistivity log, because of the insulating presence of gas hydrate in the pore space, and the sonic log, reflecting the consolidating effect of the solid crystalline compound replacing the pore fluid [*Collett*, 1998]. A very complete suite of logs was recorded during two phases of the Mallik Gas Hydrate Research program in the Mackenzie delta, Canada. Confirming the qualitative observations of *Guerin et al.* [1999], the sonic logging waveforms recorded have indicated anomalously high attenuation values associated with the presence of gas hydrate [*Guerin and Goldberg*, 2002; *Guerin et al.*, 2005]. While this has been consequently observed in various settings [*Dvorkin and Uden*, 2004], it contradicts the conventional assumption of a decrease in attenuation that would be associated with the induration and velocity increase provided by the gas hydrate crystalline structure [*Dvorkin and Uden*, 2004]. This unexpected observation shows that the influence of gas hydrate formation on the rheological properties of sediments is more complex than the simple substitution of pore fluid by a solid phase.

[5] In this paper, we adapt *Biot*'s [1956] theory to model the interaction between gas hydrate and its host sediment in order to understand the energy dissipation process. Arguably the most widely used formulation for acoustic wave propagation and energy dissipation in porous media, the Biot model is also phenomenological in nature [*Stoll and Bautista*, 1998]. Hence it offers the possibility to separate and formulate individual mechanisms and components in order to study their respective influence. *Berryman* [1980] confirmed the Biot theory, and it has been since then modified for specific purposes, including mixed lithology [*Carcione et al.*, 2000], frozen porous media [*Leclaire et al.*, 1994], and mechanisms not accounted for in the original formulation, such as cementation [*Carcione and Seriani*, 2001] or squirt flow [*Dvorkin and Nur*, 1993; *Diallo and Appel*, 2000]. Reviewing several other models, *Chand et al.* [2004] also conclude that the Biot formulation can be used to describe the properties of hydrate-bearing sediments.

[6] Following preliminary applications of the *Leclaire et al.* [1994] model [*Guerin and Goldberg*,

2002; *Guerin et al.*, 2005], we expand these results in order to weigh the influence of possible mechanisms for energy dissipation in hydrate-bearing sediments. We first consider some of the approximations and assumptions of the original model. We review the main components of the *Leclaire et al.* [1994] model (referred hereafter as the Leclaire model), and the subsequent modifications made by several authors. Second, we modify the formulation to determine the relative importance of previously neglected mechanisms: inertial coupling, cementation, friction and squirt flow. Finally, we identify the main physical components of energy dissipation in hydrate-bearing sediments through direct calibration. We compare the model results to field sonic data recorded in the Mallik 5L-38 well and discuss the implications for the deposition of gas hydrate within the sediment pore space.

2. Initial Models for Wave Propagation in Frozen Porous Media

2.1. General Theory

[7] *Biot* [1956] first formalized rigorously the propagation of acoustic waves in fluid-saturated porous media. Assuming that the principles and laws of continuum mechanics can be applied to the measurable macroscopic attributes of isotropic "effective" phases that are equivalent to the inhomogeneous components of fluid saturated sediments, *Biot* [1956] used traditional expressions for energy potentials and equations of motion to describe the displacement of the effective grain and fluid phases.

[8] *Leclaire et al.* [1994] expanded Biot's model to analyze wave propagation in frozen porous media such as frozen soil or permafrost. The effective medium is made of three phases: sediments grains, pore fluid and ice. We replace ice with gas hydrate in our formulation. In the following descriptions, the indices 1, 2 and 3 refer to the sediments as an effective solid, to the pore fluid as an effective fluid and to gas hydrate as a second effective solid. The indices s, w and h refer to the material attributes themselves: the sediment grains, the pore water and the gas hydrate. Φ_s, Φ_w and Φ_h are the volumetric fraction of each material and Φ is the formation porosity, so that $\Phi_s = 1 - \Phi$ and $\Phi_s + \Phi_w + \Phi_h = 1$.

[9] The Lagrange equations of motions combined with expressions for viscous dissipation and standard elastic stress-strain relationships between the different phases result in two equations for the longitudinal and transverse displacement potentials (φ and ψ, respectively) generated by the propagating waves [*Leclaire et al.*, 1994]:

$$\mathbf{R}\nabla\varphi = \boldsymbol{\rho}\ddot{\varphi} + \mathbf{A}\dot{\varphi} \quad \text{and} \quad \boldsymbol{\mu}\nabla\psi = \boldsymbol{\rho}\ddot{\psi} + \mathbf{A}\dot{\psi}, \tag{1}$$

where the overlaying dots indicate time derivatives and $\mathbf{R}$, $\boldsymbol{\mu}$, $\boldsymbol{\rho}$, and $\mathbf{A}$ are the matrices of rigidity, shear moduli, mass densities and friction coefficient, respectively:

$$\mathbf{R} = \begin{bmatrix} R_{11} & R_{12} & R_{13} \\ R_{12} & R_{22} & R_{23} \\ R_{13} & R_{23} & R_{33} \end{bmatrix}, \boldsymbol{\mu} = \begin{bmatrix} \mu_1 & 0 & \mu_{13} \\ 0 & 0 & 0 \\ \mu_{13} & 0 & \mu_3 \end{bmatrix},$$
$$\boldsymbol{\rho} = \begin{bmatrix} \rho_{11} & \rho_{12} & \rho_{13} \\ \rho_{12} & \rho_{22} & \rho_{23} \\ \rho_{13} & \rho_{23} & \rho_{33} \end{bmatrix}, \mathbf{A} = \begin{bmatrix} b_{11} & -b_{11} & 0 \\ -b_{11} & b_{11} + b_{33} & -b_{33} \\ 0 & -b_{33} & b_{33} \end{bmatrix}. \tag{2}$$

All parameters indexed *ij*, with $i \neq j$, refer to some form of coupling or interaction between phases *i* and *j*, while the *i* or *ii* indices indicate the attributes of the effective phase *i*. Assuming that the propagating wave and displacements are sinusoidal with a single angular frequency ω, time derivatives have the simple form of a multiplication by the constant $\mathbf{j}\omega$, where $\mathbf{j}$ is the complex square root of -1, and equation (1) can then be solved by determining the eigenvalues of the matrix $(\boldsymbol{\rho} - \mathrm{j}/\omega.\mathbf{A})$ relatively to $\mathbf{R}$ and $\boldsymbol{\mu}$. This comes to calculate the roots Λ_p and Λ_s of two polynomial equations:

$$|\boldsymbol{\rho} - (\mathbf{j}/\omega)\mathbf{A} - \Lambda_p\mathbf{R}| = 0 \quad \text{and} \quad |\rho - (\mathbf{j}/\omega)\mathbf{A} - \Lambda_s\boldsymbol{\mu}| = 0, \tag{3}$$

where $|\ldots|$ denotes the determinant of the matrices [*Leclaire et al.*, 1994]. These equations result in a third order and a second order polynomial, respectively, solvable by analytical formulas. The velocity and attenuation are then determined by identification with the definition of Λ_p and Λ_s:

$$\frac{1}{\sqrt{\Lambda_p}} = \frac{1}{V_p}\left(1 + \frac{\mathbf{j}}{2Q_p}\right) \quad \text{and} \quad \frac{1}{\sqrt{\Lambda_s}} = \frac{1}{V_s}\left(1 + \frac{\mathbf{j}}{2Q_s}\right). \tag{4}$$

When the polynomials have multiple roots, we consider only the solutions with the lowest attenuation for each mode.

2.2. Determination of the Matrix Coefficients

2.2.1. Rigidity and Shear Moduli

[10] The rigidity and shear modulus are measures of the capacity of a medium to deform under stress, which in this case is generated by the propagation of an acoustic wave. The null coefficients in the shear moduli matrix $\boldsymbol{\mu}$ result from the lack of shear strength in the pore fluid. The other generalized elastic coefficients in the rigidity and shear moduli matrices are derived from the consolidation models of *Biot and Willis* [1957] and *Johnson and Plona* [1982]:

$$R_{11} = K_1 + 4\mu_1/3 \tag{5a}$$

$$R_{22} = K_2 \tag{5b}$$

$$R_{33} = K_3 + 4\mu_3/3 \tag{5c}$$

$$R_{12} = [(1 - c_1)\Phi_s]\Phi_w K_{av} \tag{5d}$$

$$R_{23} = [(1 - c_3)\Phi_h]\Phi_w K_{av}, \tag{5e}$$

where K_i and μ_i (i = 1, 2, 3) are the bulk and shear moduli of the effective phase i defined by

$$K_1 = [(1 - c_1)\Phi_s]^2 K_{av} + K_{sm} \tag{6a}$$

$$\mu_1 = [(1 - g_1)\Phi_s]^2 \mu_{av} + \mu_{sm} \tag{6b}$$

$$K_2 = \Phi_w^2 K_{av} \tag{6c}$$

$$K_3 = [(1 - c_3)\Phi_h]^2 K_{av} + K_{hm} \tag{6d}$$

$$\mu_3 = [(1 - g_3)\Phi_h]^2 \mu_{av} + \mu_{hm}. \tag{6e}$$

K_{av} and μ_{av} are average bulk and shear moduli defined by

$$K_{av} = [(1 - c_1)\Phi_s/K_s + \Phi_w/K_w + (1 - c_3)\Phi_h/K_h]^{-1} \tag{7a}$$

$$\mu_{av} = [(1 - g_1)\Phi_s/\mu_s + \Phi_w/2\mathbf{j}\omega\eta_w + (1 - g_3)\Phi_h/\mu_h]^{-1}. \tag{7b}$$

K_{sm}, K_{hm}, μ_{sm} and μ_{hm} are the bulk and shear moduli of the dry solid and hydrate matrices, respectively. They are also referred as frame moduli. c_1, g_1, c_3 and g_3 are consolidation coefficients for the effective solid and hydrate defined in Biot's theory ($c_1 = K_{sm}/\Phi_s K_s$; $g_1 = \mu_{sm}/\Phi_s\mu_s$; $c_3 = K_{hm}/\Phi_h K_h$; $g_3 = \mu_{hm}/\Phi_h\mu_h$). The imaginary component in the expression of the average shear modulus μ_{av} represents viscous dissipation that was neglected by *Leclaire et al.* [1994] but introduced later by *Carcione and Tinivella* [2000].

[11] While *Leclaire et al.* [1994] do not use any specific formulation for the sediment frame elastic moduli, we apply the method of *Dvorkin et al.* [1999] which uses a critical porosity (Φ_c) to distinguish two regimes of consolidation. In consolidated sediments, when porosity is below the critical porosity, the expressions for the frame elastic moduli are [*Dvorkin et al.*, 1999]

$$K_{sm} = \left[\frac{\Phi/\Phi_c}{K_c + 4/3\mu_c} + \frac{1 - \Phi/\Phi_c}{K_s + 4/3\mu_c}\right]^{-1} - \frac{4}{3}\mu_c \tag{8a}$$

$$\mu_{sm} = \left[\frac{\Phi/\Phi_c}{\mu_c + Z} + \frac{1 - \Phi/\Phi_c}{\mu_s + Z}\right]^{-1} - Z, \tag{8b}$$

where K_c and G_c are the dry moduli at critical porosity:

$$K_c = \left[Pn_c^2(1 - \Phi_c)^2\mu_s^2/\left(18\pi^2(1 - \nu)^2\right)\right]^{1/3} \tag{8c}$$

$$\mu_c = 3K_c(5 - 4\nu)/[5(2 - \nu)] \tag{8d}$$

$$Z = \mu_c/6(9K_c + 8\mu_c)/(K_c + 2\mu_c). \tag{8e}$$

ν is the grain Poisson ratio ($\nu = 0.5(K_s - 2\mu_s/3)/(K_s + \mu_s/3)$), P is the effective pressure, and n_c is the average number of contacts per grain. We assume that the pore fluid pressure is hydrostatic, and that $n_c = 9$ and $\Phi_c = 38\%$ [*Dvorkin et al.*, 1999].

[12] The elastic moduli of the gas hydrate matrix K_{hm} and μ_{hm} are calculated by the percolation theory described by *Leclaire et al.* [1994], and

assuming that gas hydrate concentrations can vary between 0 and 100%:

$$K_{hm} = K_{max}(\Phi_h/\Phi)^{3.8} \text{ and } \mu_{hm} = \mu_{max}(\Phi_h/\Phi)^{3.8}, \quad (9)$$

where K_{max} and μ_{max} are calculated with the *Kuster and Toksöz* [1974] model for a gas hydrate matrix with a porosity of $(1 - \Phi)$.

2.2.2. Generalized Mass Density

[13] The generalized mass densities are used to express the kinetic energy of the effective phases, and the cross coefficients $\rho_{ij}(i \neq j)$ represent the induced mass due to the oscillation of one phase into another [*Berryman*, 1980], which results in the transfer of kinetic energy between the phases. The coefficients are derived from Biot's theory by calculating the kinetic energy density in a unit volume where energy transfers occur by inertial coupling:

$$\rho_{11} = a_{13}\Phi_s\rho_s + (a_{12} - 1)\Phi_w\rho_w + (a_{31} - 1)\Phi_h\rho_h \quad (10a)$$

$$\rho_{22} = (a_{12} + a_{23} - 1)\Phi_w\rho_w \quad (10b)$$

$$\rho_{33} = (a_{13} - 1)\Phi_s\rho_s + (a_{23} - 1)\Phi_w\rho_w + a_{31}\Phi_h\rho_h \quad (10c)$$

$$\rho_{12} = -(a_{12} - 1)\Phi_w\rho_w \quad (10d)$$

$$\rho_{23} = -(a_{23} - 1)\Phi_w\rho_w, \quad (10e)$$

where the, and a_{ij} is the inertial drag parameter of the phase i flowing through the phase j, also referred to as tortuosity [*Leclaire et al.*, 1994; *Carcione and Seriani*, 2001]:

$$a_{12} = 1 + r_{12}\Phi_s(\Phi_w\rho_w + \Phi_h\rho_h)/\rho_w\Phi_w(\Phi_w + \Phi_h) \quad (11a)$$

$$a_{23} = 1 + r_{23}\Phi_h(\Phi_w\rho_w + \Phi_s\rho_s)/\rho_w\Phi_w(\Phi_w + \Phi_s) \quad (11b)$$

where the coefficients r_{ij} reflect the geometry of the interface between phases i and j and are typically between 0 and 1 [*Berryman and Wang*, 2000].

2.2.3. Friction

[14] Friction results from the interaction of two phases in contact but with different local velocities. The friction coefficients in **A** are derived by considering that only viscous dissipation is occurring and that dissipation forces are linear functions of the difference in velocities between the phases:

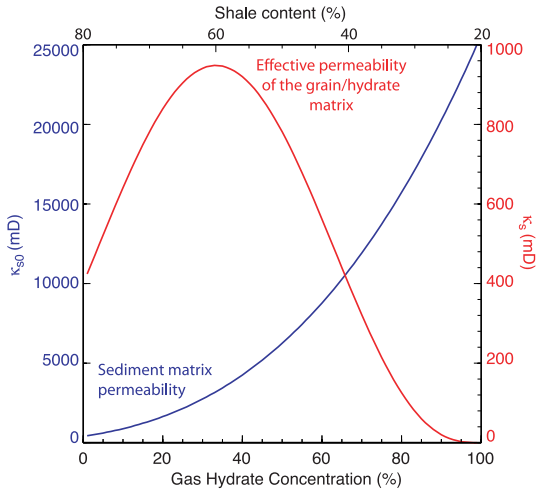

Figure 1. Permeability functions used in the model to take into account the influence of lithology on gas hydrate deposition. κ_{s0} (blue line) is the grain matrix permeability calculated with equation (14c); κ_s (red line) is the effective permeability after application of the Kozeny-Carman relationship (equation (13)) for the effect of gas hydrate concentration.

$$b_{11} = \eta_w\Phi_w^2/\kappa_s \quad \text{and} \quad b_{33} = \eta_w\Phi_w^2/\kappa_h, \quad (12)$$

where η_w is the dynamic viscosity of the pore water, and κ_s and κ_h are the effective permeability of the sediment and of the hydrate matrices, calculated from the sediment and hydrate frame permeabilities κ_{s0} and κ_{h0} by Kozeny-Carman relationships [*Leclaire et al.*, 1994]:

$$\kappa_s = \kappa_{s0}(\Phi_w/\Phi)^3 \quad \text{and} \quad \kappa_h = \kappa_{h0}(\Phi/\Phi_h)^2(\Phi_w/\Phi_s)^3. \quad (13)$$

The null coefficients in the friction matrix result from the assumption that there is no contact between solid grain and gas hydrate.

[15] In the original *Leclaire et al.* [1994] model, there is no direct interaction between ice and grains. As a result, the only energy transfer between the two solid phases is through the pore fluid, and all cross coefficients between the grain and the ice are null ($R_{13} = \mu_{13} = 0$; $\rho_{13} = 0$).

2.3. Influence of Lithology

[16] *Guerin and Goldberg* [2002] show that gas hydrate deposition is highly controlled by lithology, and that gas hydrate forms preferably in sand-rich intervals with larger pore space. Therefore we

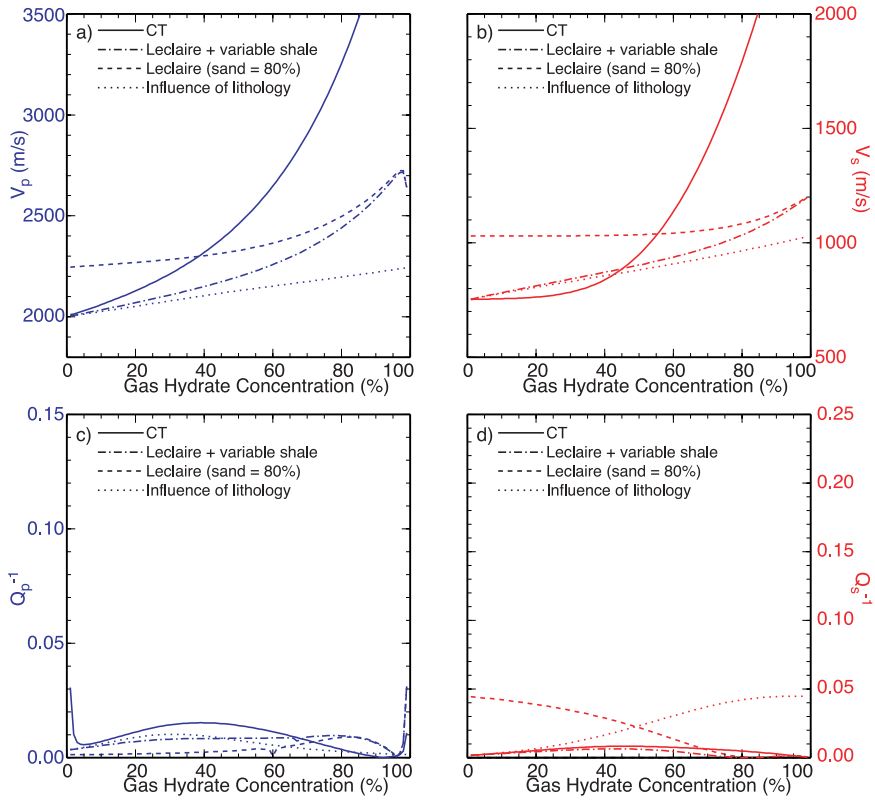

Figure 2. Results of existing models for wave propagation in gas hydrate–bearing sediments. (a) V_p; (b) V_s; (c) Q_p^{-1}; (d) Q_s^{-1}. Except when specified otherwise, these models have been modified to take into account the tendency of gas hydrate to form in sand-rich intervals. The curves labeled "Influence of lithology" represent the contribution of the lithological variability alone, obtained by varying the shale content in equations (14a)–(14c), using $\gamma = 0.80 - 0.60\Phi_h$, while keeping the gas hydrate concentration null in all other equations. See text for details. CT, Carcione and Tinivella model.

assume that the shale fraction (γ) decreases linearly while we increase gas hydrate concentration in the model. This affects only the sediments elastic moduli K_s and μ_s, calculated by a Voigt-Reuss-Hill average of the moduli of the two mineral components sand and clays [*Hamilton*, 1971], and the sediment matrix permeability κ_{s0}, which is calculated from *McCarthy* [1991]:

$$K_s = \frac{1}{2}\left[\gamma K_{clay} + (1-\gamma)K_{sand} + \frac{K_{sand}K_{clay}}{K_{sand}\gamma + K_{clay}(1-\gamma)}\right] \quad (14a)$$

$$\mu_s = \frac{1}{2}\left[\gamma \mu_{clay} + (1-\gamma)\mu_{sand} + \frac{\mu_{sand}\mu_{clay}}{\mu_{sand}\gamma + \mu_{clay}(1-\gamma)}\right] \quad (14b)$$

$$\kappa_{s0} = \kappa_{sand}(1-\gamma)^3, \quad (14c)$$

where κ_{sand} is the permeability of the clean sand.

[17] Figure 1 shows the variations in permeability as a function of hydrate concentration or shale content used in the model, assuming that the shale fraction varies between 80% and 20% of the grain (i.e., $\gamma = 0.80 - 0.60\Phi_h$) which is representative of a typical alternating sequence of terrigenous marine sediments.

2.4. Results of the Leclaire Model

[18] In Figure 2 we show the results of the Leclaire formulation for a formation containing 80% of sand, similar to common hydrate-bearing formations, and the results when assuming that the shale fraction decreases linearly with increasing hydrate concentration. In the same figure, the influence of equations (14a)–(14c) is illustrated by using the same formulation and the same linear decrease in shale content while maintaining a null gas hydrate concentration in all the other equations. The resulting curve, labeled "Influence of lithology," represents the actual contribution of lithology and of equations (14a)–(14c) to the changes in velocity

Table 1. Parameters Used in the Model

Parameter	Value
Porosity, %	35
Grain density, kg/m^3	2700
Water density, kg/m^3	1000
Hydrate density, kg/m^3	900
Sand bulk modulus, $\times 10^9$ Pa	38
Sand shear modulus, $\times 10^9$ Pa	44
Shale bulk modulus, $\times 10^9$ Pa	21.2
Shale shear modulus, $\times 10^9$ Pa	6.67
Pore fluid bulk modulus, $\times 10^9$ Pa	2.67
Hydrate bulk modulus, $\times 10^9$ Pa	7.9
Hydrate shear modulus, $\times 10^9$ Pa	3.3
Coupling shear modulus (μ_{sh0} in equation (17))	4.4×10^{10}
Sand permeability (κ_{sand}), m^2	5×10^{-11}
Hydrate permeability (κ_{io} of *Leclaire et al.* [1994]), m^2	1×10^{-5}
Grain/hydrate coefficient of friction ($b_{grain/hydrate}$), kg m^{-3} s^{-1}	2.2×10^8
Monopole source frequency, Hz	14000
Dipole source frequency, Hz	2000
Water viscosity, kg m^{-1} s^{-1}	1.8×10^{-3}

and attenuation. All the values of the parameters used are listed in Table 1 and are similar to the values used by *Helgerud et al.* [1999] and *Carcione and Tinivella* [2000].

[19] The influence of lithology is far from negligible, but represents only a ~12% increase in velocity at maximum sand and hydrate content. By comparison to the results with fixed sand content, the velocity increase due to hydrate is slightly enhanced by the inclusion of lithological changes in the Leclaire formulation. None of these results shows any significant attenuation. In fact, the results of the Leclaire model with the fixed sand content actually show a decrease in shear attenuation with increasing hydrate concentration. Using the Leclaire formulation, *Guerin and Goldberg* [2002] predicted an increase in attenuation with increasing gas hydrate concentration. The apparent contradiction with these earlier results comes from the use of extreme values for hydrate permeability and shear modulus by *Guerin and Goldberg* [2002].

2.5. Sediment–Gas Hydrate Interaction

[20] Some of the assumptions made by *Leclaire et al.* [1994] when describing frozen soil may need to be reconsidered for sediment-hydrate interaction. In particular, *Leclaire et al.* [1994] assume that there is no contact between ice and sediments, while *Guerin et al.* [1999] show that some form of cementation occurs between sediment grains and gas hydrate. *Carcione and Tinivella* [2000], *Carcione and Seriani* [2001] and *Gei and Carcione* [2003] have added grain/hydrate interaction to the Leclaire model, and were able to predict a significant increase in velocity due to the presence of gas hydrate. They introduced this interaction through the generalized elastic coefficients R_{13} and μ_{13}, and the generalized density ρ_{13} by adapting equations (5a)–(5e) and (10a)–(10e) following Biot's formulation:

$$R_{13} = (1 - c_1)(1 - c_3)\Phi_s\Phi_h K_{av} + 2\mu_{13}/3 \tag{15a}$$

$$\mu_{13} = (1 - g_1)(1 - g_3)\Phi_s\Phi_h\mu_{av} + \mu_{sh} \tag{15b}$$

$$\rho_{13} = -(a_{13} - 1)\Phi_s\rho_s - (a_{31} - 1)\Phi_h\rho_h \tag{15c}$$

with

$$a_{13} = 1 + r_{13}\Phi_h(\Phi_s\rho_s + \Phi_h\rho_h)/\rho_s\Phi_s(\Phi_s + \Phi_h) \tag{15d}$$

$$a_{31} = 1 + r_{31}\Phi_s(\Phi_s\rho_s + \Phi_h\rho_h)/\rho_h\Phi_h(\Phi_s + \Phi_h). \tag{15e}$$

[21] *Carcione and Tinivella* [2000] include cementation by considering that gas hydrate is part of the solid matrix and use a percolation model to define the sediment matrix shear modulus μ_{sm}, instead of using equation (8b):

$$\mu_{sm} = (\mu_{smKT} - \mu_{sm0})(\Phi_h/\Phi)3.8 + \mu_{sm0}, \tag{16}$$

where μ_{smKT} is the matrix shear modulus estimated by *Kuster and Toksöz* [1974] and μ_{sm0} is the rigidity of the sediments at full water concentration. The coupling shear modulus between sediments and gas hydrate, μ_{sh} in equation (15b), is

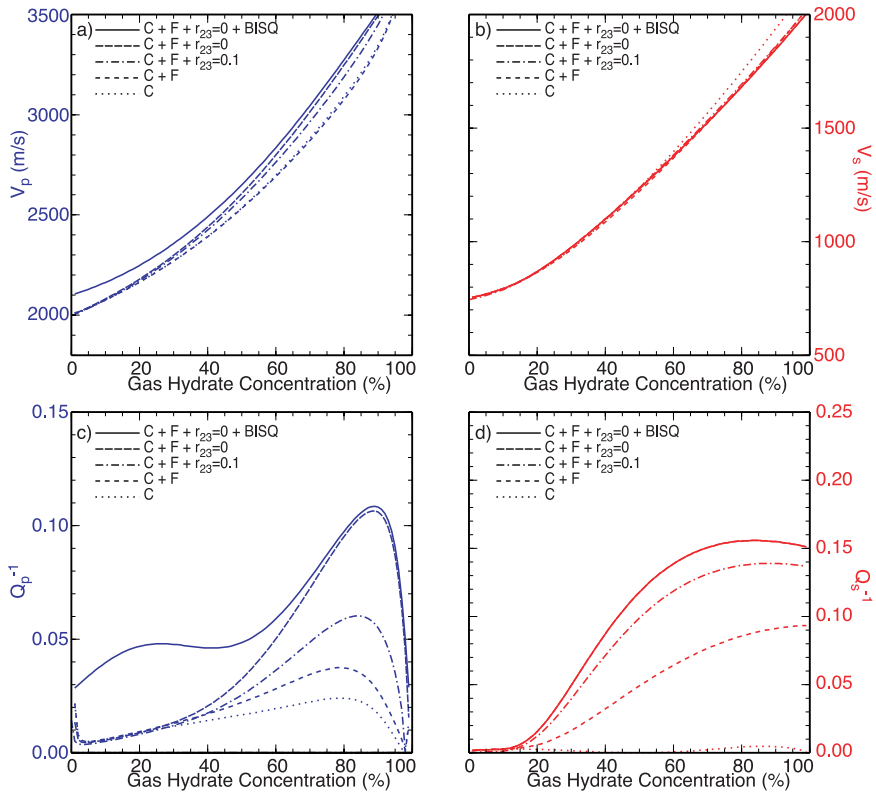

Figure 3. Results of the successive modifications of the model for wave propagation in gas hydrate–bearing sediments, including the addition of cementation, friction, and squirt flow, and changes in the inertial coupling parameter r_{23}. (a) V_p; (b) V_s; (c) Q_p^{-1}; (d) Q_s^{-1}. Abbreviations for the models: C, cementation; F, friction; BISQ, Squirt Flow. The value of the coefficient r_{23} is null when hydrate/pore fluid inertial coupling is absent. If not specified, $r_{23} = 0.5$.

null in this model. Results of the *Carcione and Tinivella* [2000] model (hereafter referred as CT) are compared to the Leclaire results in Figure 2. The increase in velocity with increasing hydrate concentration in the CT model is significantly higher than in the Leclaire model, but this formulation still fails to predict any significant attenuation. In addition, the shear velocity curve suggests only a negligible increase when hydrate concentration is less than ~30%, and a very steep increase for higher concentrations. In situ V_s data from the Blake Ridge show that V_s increases at much lower hydrate concentrations [*Guerin et al.*, 1999].

3. Improvement to Existing Models

3.1. Cementation

[22] Instead of considering gas hydrate as a part of the solid matrix, we assume that the *Dvorkin et al.* [1999] formulation (equations (8a)–(8e)) describes accurately the sediment matrix μ_{sm}, and that cementation between gas hydrate and sediments can be described by the coupling shear modulus μ_{sh} (equation (15b)). Using an expression similar to the shear moduli in the consolidation models of *Johnson and Plona* [1982], a simple expression for this modulus is a 2nd order polynomial function of the grain and gas hydrate fractions:

$$\mu_{sh} = \mu_{sh0}(\Phi_h\Phi_s)^2 = \mu_{sh0}(\Phi_h(1-\Phi))^2. \qquad (17)$$

Without an existing value for μ_{sh0}, the value of this parameter was determined iteratively in order to reproduce a final V_p value at maximum hydrate concentration similar to the CT results. The results, labeled "C" in Figure 3, show that this modification predicts a more gradual increase in V_s than the CT model, a slightly enhanced increase in compressional attenuation (Q_p^{-1}), but no shear wave attenuation.

3.2. Friction

[23] *Leclaire et al.* [1994] assume that there is no contact between the solid phases and do not include any friction between sediments and ice. *Carcione and Tinivella* [2000], *Carcione and Seriani* [2001], and *Gei and Carcione* [2003] consider some grain/hydrate interaction but also neglect friction. Having established that cementation between grains and gas hydrate is necessary to reproduce the velocity increase with hydrate concentration [*Guerin et al.*, 1999], some contact, and presumably some friction, is also likely to occur between these two phases. *Berryman and Wang* [2000] describe friction between solid phases for double-porosity, double-permeability media. We assume that the frictional forces between solid grains and hydrate are linear functions of the velocity differential between them, similar to the viscous frictional forces against pore fluid. We define a new friction coefficient b_{13} as a 2nd order polynomial function of the gas hydrate and sediment fractions, similar to the expressions for b_{11} and b_{33}, and to the drag coefficients calculated by *Berryman and Wang* [2000]. The resulting expressions for the friction matrix $\mathbf{A}$ is

$$\mathbf{A} = \begin{bmatrix} b_{11}+b_{13} & -b_{11} & -b_{13} \\ -b_{11} & b_{11}+b_{33} & -b_{33} \\ -b_{13} & -b_{33} & b_{33}+b_{13} \end{bmatrix}$$
$$\text{with } b_{13} = b_{13}^0(\Phi_h(1-\Phi))^2. \tag{18}$$

Adding friction to the results in Figure 3 generates a higher compressional attenuation Q_p^{-1} than in any previous model and a clear increase in shear attenuation with gas hydrate concentration. We suggest that friction between gas hydrate and sediment grains could be responsible for the shear energy dissipation observed in previous studies.

3.3. Inertial Coupling

[24] By adding friction and cementation to the existing models, several new parameters must be defined. In particular, we determined iteratively the value of b_{13}^0, as given in Table 1, in order to predict the maximum effect of gas hydrate concentration on attenuation. In addition to these new parameters, existing theoretical parameters can be reconsidered. The tortuosity a_{ij} and the inertial coupling coefficients r_{ij} define the geometrical aspect of the physical boundary separating phases. They correspond to a theoretical porous medium with well defined grain and pore geometries and can be in fact treated arbitrarily considering the heterogeneity of sediment grains and gas hydrate. *Leclaire et al.* [1994] use a value of 0.5 for the geometrical aspect of the ice/water interface, r_{23}, and *Carcione and Seriani* [2001] suggest a value of $r_{13} = r_{31} = 0$ for the grain/hydrate interface. We have used these values in all previous results, but we observe that decreasing r_{23} increases the predicted attenuation significantly. Figure 3 shows the results for $r_{23} = 0.1$ and $r_{23} = 0$, that can be compared to the results with the original value ($r_{23} = 0.5$). The highest values for Q_p^{-1} and Q_s^{-1} are obtained for $r_{23} = 0$, suggesting that there is little, if any, inertial coupling between gas hydrate and the pore water.

3.4. Squirt Flow

[25] Although the results in Figure 3 predict an increase in attenuation with increasing hydrate concentration, generated by the combined physical mechanisms described above, none of these results predicts any attenuation at low hydrate concentration. Except for the viscous friction with the pore fluid included in equation (7b), there is no energy dissipation mechanisms independent from the presence of hydrate. *Leclaire et al.* [1994] and *Carcione and Seriani* [2001] consider energy dissipation only in the direction of wave propagation. *Dvorkin and Nur* [1993] proposed the BISQ (Biot/Squirt) flow theory, where squirt flow is added to the Biot formulation, and fluid is squeezed laterally from pores that are deformed by a passing elastic wave. *Diallo and Appel* [2000] proposed a modification to the BISQ model, describing squirt flows without requiring the "squirt length" parameter to be arbitrarily defined. To introduce squirt flow into the Leclaire model, we replace the pore fluid stress/strain relationship by expanding the *Diallo and Appel* [2000] formulation of pore pressure for a three-phase medium. Thus we replace the expressions for the elastic coefficients related to the pore fluid in the rigidity matrix R_{12}, R_{23} and R_{22} and transform equations (5b), (5d), and (5e) to be

$$R_{22} = f_1\Phi_1 + f_3\Phi_3 \tag{19a}$$

$$R_{12} = f_1(\alpha_1 - \Phi_1) \tag{19b}$$

$$R_{23} = f_3(\alpha_3 - \Phi_3) \tag{19c}$$

with

$$\Phi_1 = \frac{\Phi_w}{1-\Phi_h}; \alpha_1 = \frac{1}{3}\left(1 - \frac{K_{sm}}{K_s} + 2\Phi_1\right);$$
$$f_1 = \left(\frac{1}{K_w} + \frac{1}{\Phi_1 Q_1}\right)^{-1}; Q_1 = \frac{K_s}{1 - \Phi_1 - K_{sm}/K_s}$$

$$\Phi_3 = \frac{\Phi_w}{\Phi}; \alpha_3 = \frac{1}{3}\left(1 - \frac{K_{hm}}{K_h} + 2\Phi_3\right);$$
$$f_3 = \left(\frac{1}{K_w} + \frac{1}{\Phi_3 Q_3}\right)^{-1}; \text{and } Q_3 = \frac{K_h}{1 - \Phi_3 - K_{hm}/K_h}.$$

Figure 3 shows that the addition of squirt flow increases the compressional attenuation at low gas hydrate concentration. At higher concentrations, as the effective permeability κ_s decreases (see Figure 1), the contribution of squirt flow becomes negligible. Because the pore fluid does not transmit shear energy, the addition of squirt flow has no effect on shear attenuation. Hence, in Figure 3d, the Q_s^{-1} curves with $r_{23} = 0$, with and without squirt flow, overlay perfectly and only one curve is visible. However, Figure 3d still predicts a significant increase in shear attenuation at relatively low hydrate concentration (>15%). In summary, the combination of the friction, cementation, and squirt flow mechanisms, without inertial coupling, in the three-phase Leclaire formulation predicts increases in velocity and attenuation with increasing gas hydrate concentration, even at low hydrate concentrations.

4. Sonic Waveform Attenuation in Mallik 5L-38

[26] We developed this composite model to reproduce the sonic logs observations by *Guerin et al.* [1999] and *Guerin and Goldberg* [2002]. To evaluate its accuracy and predict the relative influence of the different mechanisms on energy dissipation, we now compare the model results with the logging data recorded in the Mallik 5L-38 well.

[27] *Dallimore and Collett* [2005] describe the achievements of the 2002 Mallik Gas Hydrate Research program in detail. Monopole and dipole sonic logging waveforms were recorded in the Mallik 5L-38 well in 2002 and in the Mallik 2L-38 well in 1999. Low amplitude sonic waveforms were observed in these data in all the hydrate-rich intervals [*Guerin et al.*, 2005; *Guerin and Goldberg*, 2002]. Figures 4a and 4f show the monopole and dipole waveform amplitudes recorded by two of the tool's eight receivers. To quantify the energy dissipation, we calculated the intrinsic attenuation, or energy loss per waveform cycle, using the median frequency shift method developed by *Frazer et al.* [1997] and *Sun et al.* [2000] and described by *Guerin and Goldberg* [2002]. In Figures 4b and 4e we compare these values with the results from the more traditional spectral ratio method [*Goldberg et al.*, 1984]. While the results of spectral ratios method are more noisy, because this method is unstable and extremely sensitive to variations in hole and formation parameters [*Sams and Goldberg*, 1990], the two methods agree overall and indicate an increase in intrinsic attenuation in the intervals where gas hydrate has been identified. Because the values calculated with the *Frazer et al.* [1997] approach are significantly less noisy, only these values are discussed further. Intervals with high attenuation clearly coincide with the low amplitudes in the waveforms. These intervals, highlighted in Figures 4b–4e, are also characterized by higher sonic velocity (Figure 4d), and correspond to the intervals where Archie's method applied to the resistivity log [*Guerin et al.*, 2005] indicate high gas hydrate concentration (Figure 4c).

4.1. Influence of Lithology in Mallik 5L-38

[28] In Figure 4c, the gamma ray log and the gas hydrate concentration curve shows that all intervals with high hydrate concentration, within the gas hydrate stability zone, occur in sands, indicated by low gamma ray values. Figure 5 shows the gamma ray data plotted against gas hydrate concentration in the Mallik 5L-38 well. High Gamma Ray values indicate shaly content. While low (<20%) gas hydrate concentrations can be observed over the entire range of gamma-ray values, a negative correlation between shale content and gas hydrate concentration is clear for higher hydrate concentrations, supporting the model assumption of a linear relationship between shale content and hydrate concentration.

4.2. Comparison of Models and Data

[29] Figure 6 shows a comparison of some of the model results with crossplots of the sonic velocities and attenuations against gas hydrate concentration measured in the Mallik 5L-38 well. Despite significant scattering, the data show a strong positive correlation between gas hydrate concentration, velocity and attenuation.

[30] The velocity and attenuation increases with gas hydrate concentration predicted by the Leclaire

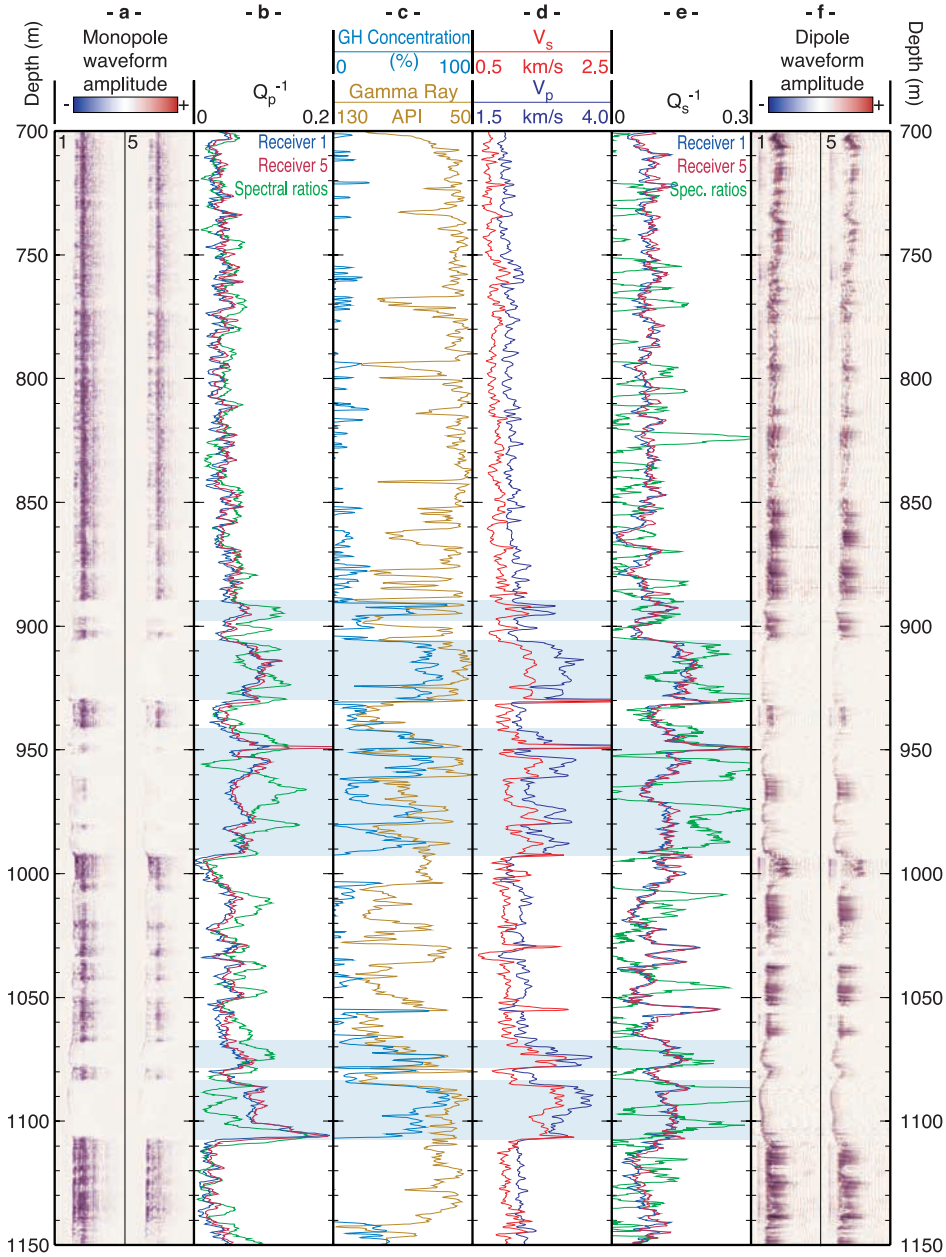

Figure 4. Downhole logs and sonic waveforms recorded in the Mallik 5L-38 well. (a) Monopole waveforms at receivers 1 and 5. (b) Compressional attenuation (Q_p^{-1}) calculated with the *Frazer et al.* [1997] method for receivers 1 and 5 and by spectral ratios. (c) Gamma ray and gas hydrate (GH) concentration. The inverted scale for gamma ray illustrates the correlation between sand layers (low gamma ray) and high hydrate concentration. (d) V_p and V_s. (e) Shear attenuation (Q_s^{-1}) calculated with the *Frazer et al.* [1997] method for receivers 1 and 5 and by spectral ratios. (f) Dipole waveforms at receivers 1 and 5. Intervals with high hydrate concentration are underlined in blue.

model, including the lithologic effects, are significantly lower than observed in the data. The CT model agrees well for V_p, but not for V_s. The predicted trend for V_s shows almost no increase below ~30% hydrate concentration, and a steep increase for higher concentrations, while the data suggest a steady increase in V_s with hydrate concentration increasing from 0 to ~80%. *Guerin et al.* [1999] identified a similar behavior in data from the Blake ridge, where the low gas hydrate concentrations clearly increase the V_s measurements. Furthermore, neither the Leclaire nor the

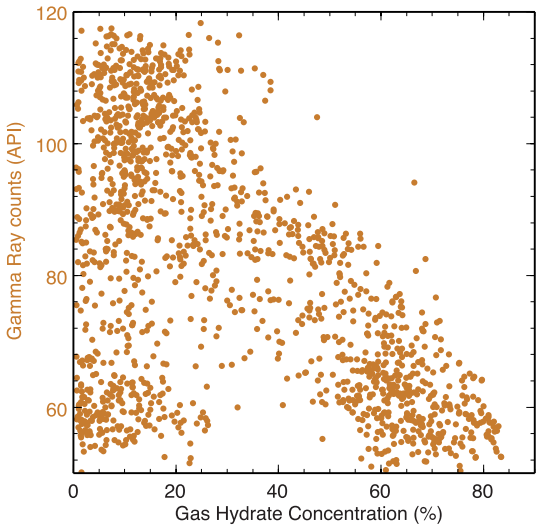

Figure 5. Relationship between gamma ray counts and gas hydrate concentration measured in Mallik 5L-38.

CT models predict attenuation increases as observed in the data from the Mallik 5L-38 well. However, by including cementation, friction and squirt flow mechanisms, and removing inertial coupling between gas hydrate and pore fluid (r_{23} = 0) in the model formulation, we are able to reproduce reasonably well the increase in both velocity and attenuation with increasing hydrate concentration. All of these mechanisms are needed to describe the velocity and attenuation of elastic waves propagating in hydrate-bearing formations. The comparison with the data also shows that to fully describe elastic wave propagation in gas hydrate–bearing sediments, it is necessary to consider both velocity and attenuation. Considering velocity alone, a comparison with the data could not discriminate the influence of friction, squirt flow or inertial coupling (see Figure 3).

[31] Despite showing a satisfactory increase in attenuation as a function of gas hydrate concentration, the model results show overall lower attenuation values than the measured data. This inability to match the observed data comes in part from the homogenization implied in the theoretical model, which does not take into account the intrinsic heterogeneity of a sedimentary formation. The assumption of a homogenous formation, and in particular the assumption of uniform porosity,

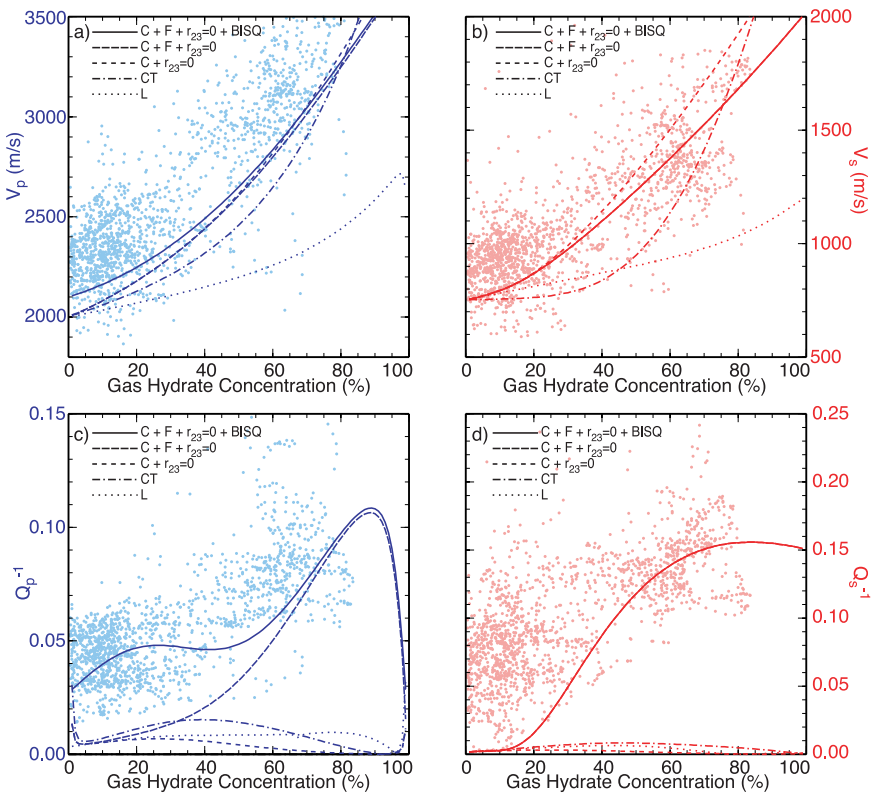

Figure 6. Comparison of the main model results with the Mallik 5L-38 data. (a) V_p; (b) V_s; (c) Q_p^{-1}; (d) Q_s^{-1}. Abbreviations for the models: L, Leclaire with varying shale; CT, Carcione and Tinivella model; C, cementation; F, friction; BISQ, Squirt Flow. The value of the coefficient r_{23} is null when hydrate/pore fluid inertial coupling is absent. If not specified, r_{23} = 0.5.

make it impossible to reproduce the dissipative effects of heterogeneous particle sizes and distribution, that are mainly responsible for the higher values and for the scattering of the data.

5. Discussion

[32] A primary result of this study is the prediction of an increase in sonic waves attenuation with increasing gas hydrate concentration. *Gei and Carcione* [2003] use the CT formulation to predict a decrease in attenuation with increasing hydrate concentration. In a review of recent works, *Dvorkin and Uden* [2004] note the apparent contradiction between the induration due to the presence of hydrate and the increase in attenuation observed by several authors, but recognize the validity of the attenuation measurements. In a theoretical study only, *Gei and Carcione* [2003] could not identify the role of elastic shear coupling, cementation, and of the friction between sediment grains and gas hydrate. The contribution of friction to energy loss at the pore scale is important because it implies that grain-hydrate cementation is only partial, strong enough to enhance shear velocity at low gas hydrate concentration, but weak enough to allow energy dissipation by relative motion and friction between the two solid phases. The elastic heterogeneity due to the very distinct elastic properties of sediment grains and gas hydrate supports the frictional forces between them.

[33] These results suggest that the main component of energy loss in hydrate-bearing sediments is the pore-scale friction between the solid phases. This seems to disagree with the conclusion of *Bourbié et al.* [1987] that intergranular friction does not contribute significantly to seismic attenuation. To the contrary, it actually underlines that the interaction between gas hydrate and the sediment grains is fundamentally different from intergranular interaction, which was first suggested by the apparent contradiction between the increase in velocity and in attenuation associated with gas hydrate presence, which triggered this work.

[34] Squirt flow and the absence of inertial coupling between gas hydrate and the pore fluid, both previously ignored, also play a significant role in predicting energy dissipation in hydrates. Figure 6 illustrates the combination of the different physical mechanisms. The best fit results are clearly the results of the composite model ($C + F + r_{23} = 0 +$ BISQ). Figure 6 also indicates that including cementation and eliminating inertial coupling without considering friction between gas hydrate and grains (model labeled $C + r_{23} = 0$) does not predict any P or S wave attenuation. It shows that without sediment/hydrate friction there is almost no attenuation. Thus the influence of the absence of inertial coupling is only secondary to friction between gas hydrate and sediments, as the primary mode for energy dissipation in hydrate-bearing sediments.

[35] *Benavente et al.* [2002] and *de Lima* [1995] note that the tortuosity of a porous medium is inversely related to its permeability. The high permeability of the hydrate matrix, particularly in comparison to the permeability of the sediment frame (see Table 1), implies a low tortuosity. Therefore the hydrate matrix offers only a limited inertial resistance to fluid motion and allows little inertial coupling between gas hydrate and the pore fluid. This suggests that there is no oscillation of gas hydrate within the pore fluid [*Berryman and Wang*, 2000] and that gas hydrate is not moving freely within the pore space but rather deposited on the grains. It is consistent with the existence of the strong cementation which is mainly responsible for the shear velocity increase. *Bedford et al.* [1984] and *Leclaire et al.* [2001] discuss the relative influence of viscous and inertial forces in porous media. *Leclaire et al.* [2001] argue that these two forces are mutually exclusive of each other. Hence the absence of inertial coupling between gas hydrate and pore fluid suggests that energy dissipation between these two phases occurs only through viscous friction. The Leclaire and CT models both include viscous fluid friction and fail to generate any significant attenuation (Figure 2). Therefore the only significant energy loss mechanism at low hydrate concentrations is the squirt flow.

[36] The first indication of energy dissipation associated with the presence of gas hydrate, which initiated our interest for this study, was the ''blanking'' effect observed in several gas hydrate deposits. However, in order to achieve deep penetration, seismic sources have lower frequencies (~10–500 Hz) than sonic logs. In Figure 7, we show the results of our model showing the influence of gas hydrate on attenuation as a function of the acoustic source frequency. At high frequency and low gas hydrate concentration, higher Q_p^{-1} values reflect the dominant effect of squirt flow at the pore scale at low concentrations (Figure 7a). The frequency dependence of this mechanism is in agreement with the results of *Diallo and Appel* [2000] and *Sams et al.* [1997]. Figure 7 also indicates an increase in attenuation with gas hydrate concentration for all

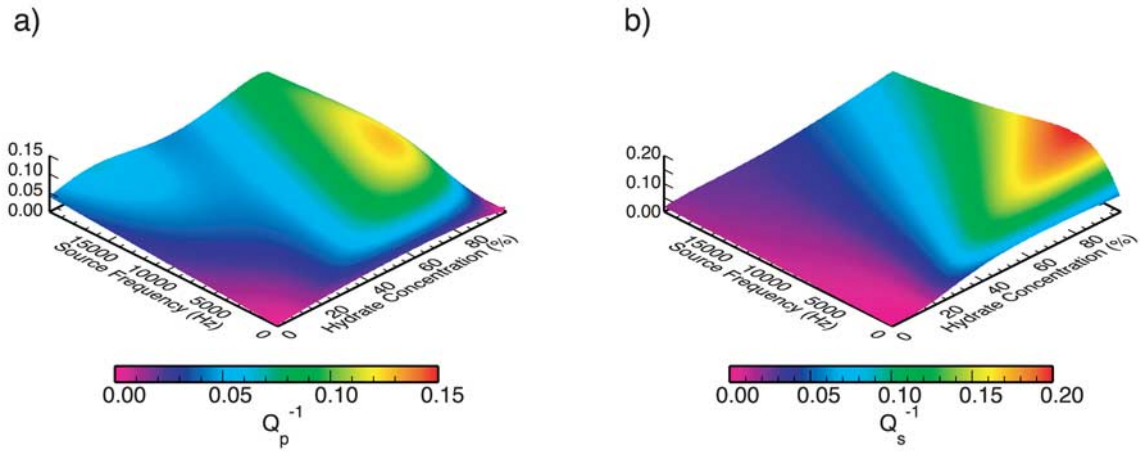

Figure 7. Analysis of the influence of the sonic source frequency on the model results for (a) compressional attenuation and (b) shear attenuation.

sonic source frequencies, with peak values in the 5–10 kHz range for Q_p^{-1} and between 0.5–5 kHz for Q_s^{-1}. Hence, while the influence of gas hydrate on attenuation is measurable over all frequencies, the strongest effect in the seismic frequency range is on the shear attenuation. Observations by *Bauer et al.* [2005] and *Pratt et al.* [2005] for crosshole seismic data and by *Sakai* [1999] for shear wave VSP data provide consistent evidences for this conclusion. High attenuation at seismic frequencies may explain the "blanking," and these results could possibly be used to estimate gas hydrate concentrations at larger scale, provided that gas hydrate is distributed somehow uniformly along the seismic wave path. This assumption is probably valid in thick hydrate intervals, such as in Mallik 5L-83, but not in patchy or heterogeneous gas hydrate distribution such as on the Blake Ridge. In such environments, seismic energy loss mechanisms similar to those discussed here must occur but cannot be quantified without consideration of their discontinuous and anisotropic nature.

6. Conclusion

[37] These results confirm that a modified Biot theory can describe acoustic wave propagation in gas hydrate–bearing sediments, provided that physical interactions are considered between all solid and fluid phases, including cementation and friction between gas hydrate and the sediment matrix. In our formulation, an increase in shear velocity at low gas hydrate concentrations is predicted by elastic coupling due to grain-hydrate cementation that can be formalized by including a coupling shear modulus μ_{sh} in the model. The high attenuation that has been observed in hydrate deposits is attributed to several mechanisms. The primary cause of energy dissipation is grain-hydrate viscous friction due to the elastic heterogeneity between hydrate and grains. Additional attenuation (Q_p^{-1}) at low hydrate concentration is attributed to a squirt flow mechanism, which is increased by the presence of gas hydrate. We also determine that an absence of inertial coupling between gas hydrate and the pore fluid is likely, which enhances the dissipating effect of friction between gas hydrate and the sediment grains.

Acknowledgments

[38] We are grateful to Tim Collett and Scott Dallimore, who gave us the opportunity to work on this exceptional data set. Michael Buckingham, an anonymous reviewer, and the editors provided very useful comments to improve the quality and the general relevance of this manuscript. This is Lamont-Doherty Earth Observatory contribution 6797.

References

Bauer, K., R. G. Pratt, M. H. Weber, C. Haberland, T. Ryberg, and S. Shimizu (2005), Introduction and initial data analysis of the Mallik 2002 crosshole seismic experiments, in *Scientific Results From the Mallik 2002 Gas Hydrate Production Research Well Program, Mackenzie Delta, Northwest Territories, Canada*, edited by S. R. Dallimore and T. S. Collett, *Bull. Geol. Surv. Can.*, in press.

Bedford, A., R. D. Costley, and M. Stern (1984), On the drag and virtual mass coefficients in Biot's equations, *J. Acoust. Soc. Am.*, *76*(6), 1804–1809.

Benavente, D., P. Lock, M. A. G. del Cura, and S. Ordonez (2002), Predicting the capillary imbibition of porous rocks from microstructure, *Transp. Porous Media*, *49*, 59–76.

Berryman, J. G. (1980), Confirmation of Biot's theory, *Appl. Phys. Lett.*, *37*(4), 382–384.

Berryman, J. G., and H. F. Wang (2000), Elastic wave propagation and attenuation in a double-porosity dual-permeability medium, *Int. J. Rock Mech. Min. Sci.*, *37*, 63–78.

Biot, M. A. (1956), Theory of propagation of elastic waves in a fluid saturated porous solid, *J. Acoust. Soc. Am.*, *28*, 168–191.

Biot, M. A., and D. G. Willis (1957), The elastic coefficients of the theory of consolidation, *J. Appl. Mech.*, *24*, 594–601.

Bourbié, T., O. Coussy, and B. Zinszner (1987), *Acoustics of Porous Media*, 334 pp., Educ. Technol., Paris.

Carcione, J. M., and G. Seriani (2001), Wave simulation in frozen porous media, *J. Comput. Phys.*, *170*, 676–695.

Carcione, J. M., and U. Tinivella (2000), Bottom-simulating reflectors: Seismic velocities and AVO effects, *Geophysics*, *65*, 54–67.

Carcione, J. M., B. Gurevich, and F. Cavallini (2000), A generalized Biot-Gassmann model for the acoustic properties of shaley sandstones, *Geophys. Prospect.*, *48*, 539–557.

Chand, S., T. A. Minshull, D. Gei, and J. M. Carcione (2004), Elastic velocity models for gas-hydrate-bearing sediments—A review, *Geophys. J. Int.*, *159*, 573–590.

Collett, T. S. (1998), Well log evaluation of gas hydrate saturations, *Trans. SPWLA Annu. Logging Symp.*, *39th*, paper MM.

Dallimore, S. R., and T. S. Collett (Eds.) (2005), *Scientific Results From the Mallik 2002 Gas Hydrate Production Research Well Program, Mackenzie Delta, Northwest Territories, Canada*, *Bull. Geol. Surv. Can.*, in press.

de Lima, O. A. L. (1995), Water concentration and permeability from resistivity, dielectric, and porosity logs, *Geophysics*, *60*(6), 1756–1764.

Diallo, M. S., and E. Appel (2000), Acoustic wave propagation in saturated porous media: Reformulation of the Biot/Squirt flow theory, *J. Appl. Geophys.*, *44*, 313–325.

Dvorkin, J., and A. Nur (1993), Dynamic poroelasticity: A unified model with the squirt flow and the Biot mechanism, *Geophysics*, *58*, 524–533.

Dvorkin, J., and R. Uden (2004), Seismic wave attenuation in a methane hydrate reservoir, *Leading Edge*, *23*, 730–732.

Dvorkin, J., M. Prasad, A. Sakai, and D. Lavoie (1999), Elasticity of marine sediments: Rock physics modeling, *Geophys. Res. Lett.*, *26*(12), 1781–1784.

Frazer, L. N., X. Sun, and R. H. Wilkens (1997), Changes in attenuation with depth in an ocean carbonate section: ODP sites 806 and 807, Ontong Java plateau, *J. Geophys. Res.*, *102*, 2983–2997.

Gei, D., and J. M. Carcione (2003), Acoustic properties of sediments saturated with gas hydrate, free gas and water, *Geophys. Prospect.*, *51*, 141–157.

Goldberg, D., T. K. Kan, and J. P. Castagna (1984), Attenuation measurements from sonic log waveforms, *Trans. SPWLA Annu. Logging Symp.*, *25th*, paper N.

Guerin, G., and D. Goldberg (2002), Sonic waveform attenuation in gas hydrate-bearing sediments from the JAPEX/JNOC/GSC Mallik 2L-38 research well, Mackenzie Delta, Canada, *J. Geophys. Res.*, *107*(B5), 2088, doi:10.1029/2001JB000556.

Guerin, G., D. Goldberg, and A. Meltser (1999), Characterization of in situ elastic properties of gas hydrate-bearing sediments on the Blake Ridge, *J. Geophys. Res.*, *104*, 17,781–17,796.

Guerin, G., D. Goldberg, and T. S. Collett (2005), Sonic attenuation in the Mallik 5L38 gas hydrate research well, in *Scientific Results From the Mallik 2002 Gas Hydrate Production Research Well Program, Mackenzie Delta, Northwest Territories, Canada*, edited by S. R. Dallimore and T. S. Collett, *Bull. Geol. Surv. Can.*, in press.

Hamilton, E. L. (1971), Elastic properties of marine sediments, *J. Geophys. Res.*, *76*, 579–601.

Helgerud, M. B., J. Dvorkin, A. Nur, A. Sakai, and T. S. Collett (1999), Elastic-wave velocity in marine sediments with gas hydrates: Effective medium modeling, *Geophys. Res. Lett.*, *26*(13), 2021–2024.

Henriet, J. P., , and J. Mienert (Eds.) (1998), *Gas Hydrates: Relevance to World Margin Stability and Climate Change*, *Geol. Soc. Spec. Publ.*, *137*.

Holbrook, W. S., H. Hoskins, W. T. Wood, R. A. Stephen, D. Lizarralde, and Leg 164 Science Party (1996), Methane hydrate and free gas on the Blake Ridge from vertical seismic profiling, *Science*, *273*, 1840–1843.

Hornbach, M. J., W. S. Holbrook, A. R. Gorman, K. L. Hackwith, D. Lizzaralde, and I. Pecher (2003), Direct seismic detection of methane hydrate on the Blake Ridge, *Geophysics*, *68*(1), 92–109.

Johnson, D. L., and T. J. Plona (1982), Acoustic slow waves and the consolidation transition, *J. Acoust. Soc. Am.*, *72*, 556–565.

Kuster, G. T., and M. N. Toksöz (1974), Velocity and attenuation of seismic waves in two-phase media, 1, Theoretical formulation, *Geophysics*, *39*, 587–606.

Kvenvolden, K. A. (1998), A primer on the geological occurrence of gas hydrate, in *Gas Hydrates: Relevance to World Margin Stability and Climate Change*, edited by J. P. Henriet and J. Mienert, *Geol. Soc. Spec. Publ.*, *137*, 9–30.

Kvenvolden, K. A. (1999), Potential effects of gas hydrate on human welfare, *Proc. Natl. Acad. Sci. U. S. A.*, *96*, 3420–3426.

Kvenvolden, K. A. (2002), Methane hydrate in the global organic carbon cycle, *Terra Nova*, *14*, 302–306.

Leclaire, P., F. Cohen-Tenoudji, and J. Aguirre-Puente (1994), Extension of Biot's theory of wave propagation to frozen porous media, *J. Acoust. Soc. Am.*, *96*(6), 3753–3768.

Leclaire, P., K. V. Horoshenkov, and A. Cummings (2001), Transverse vibrations on a thin rectangular porous plate saturated by a fluid, *J. Sound Vibrations*, *247*(1), 1–18.

Lee, M. W., and W. P. Dillon (2001), Amplitude blanking related to the pore-filling of gas hydrate in sediments, *Mar. Geophys. Res.*, *22*, 101–109.

McCarthy, J. F. (1991), Analytical models of the effective permeability of sand-shale reservoirs, *Geophys. J. Int.*, *105*, 513–527.

Milkov, A. V., G. E. Claypool, Y.-J. Lee, W. Xu, G. R. Dickens, W. S. Borowski, and ODP Leg 204 Scientific Party (2003), In situ methane concentrations at Hydrate Ridge, offshore Oregon: New constraints on the global gas hydrate inventory from an active margin, *Geology*, *31*(10), 833–836.

Pratt, R. G., F. Hou, K. Bauer, and M. H. Weber (2005), Waveform tomography images of velocity and inelastic attenuation from the Mallik 2002 crosshole seismic surveys, in *Scientific Results From the Mallik 2002 Gas Hydrate*

Production Research Well Program, Mackenzie Delta, Northwest Territories, Canada, edited by S. R. Dallimore and T. S. Collett, *Bull. Geol. Surv. Can.*, in press.

Sakai, A. (1999), Velocity analysis of vertical seismic profile (VSP) survey at JAPEX/JNOC/GSC Mallik 2L-38 gas hydrate research well, and related problems for estimating gas hydrate concentration, in *Scientific Results From JAPEX/JNOC/GSC Mallik 2L-38 Gas Hydrate Research Well, Mackenzie Delta, Northwest Territories, Canada*, edited by S. R. Dallimore, T. Uchida, and T. S. Collett, *Bull. Geol. Surv. Can.*, *544*, 323–340.

Sams, M. S., J. P. Neep, M. H. Worthington, and M. S. King (1997), The measurement of velocity dispersion and frequency-dependent intrinsic attenuation in sedimentary rocks, *Geophysics*, *62*, 1456–1464.

Sams, M., and D. Goldberg (1990), The validity of Q estimates from borehole data using spectral ratios, *Geophysics*, *55*, 97–101.

Sloan, D. E. (1990), *Clathrate Hydrates of Natural Gases*, CRC Press, Boca Raton, Fla.

Stoll, R. D., and E. O. Bautista (1998), Using the Biot theory to establish a baseline geoacoustic model for seafloor sediments, *Cont. Shelf Res.*, *18*, 1839–1857.

Sun, X., X. Tang, C. H. Cheng, and L. N. Frazer (2000), P- and S-wave attenuation logs from monopole sonic data, *Geophysics*, *65*(2), 755–765.